Room Temperature Dye Glasses: A Guideline Toward the Fabrication of Amorphous Dye Films with Monomeric Absorption and Emission

CHEMISTRY OF MATERIALS

pubs.acs.org/cm

Article

Room Temperature Dye Glasses: A Guideline Toward the Fabrication of Amorphous Dye Films with Monomeric Absorption and Emission

Clara Schäfer, Sandra Hultmark, Yizhou Yang, Christian Müller, and Karl Börjesson*

Cite This: https://doi.org/10.1021/acs.chemmater.2c02761

Read Online

ACCESS | Metrics & More | Article Recommendations | Supporting Information

ABSTRACT: The morphology of films containing photoactive materials is crucial for the performance of solid-state dye applications. Organic dyes tend to crystallize due to their usually planar molecular structure and the resulting intermolecular interactions. This leads to inhomogeneous films with crystalline, aggregated, and amorphous regions, decreasing device efficiency and complicating spectral analysis. Improving the glass-forming ability of organic dyes therefore presents a major challenge for solid-state dye applications. Here, we present a guideline to create organic dye glasses using BODIPY as a model dye. The method is based on the strategic design of BODIPY derivatives, equipped with short alkyl chains, in combination with blending of two or more derivatives. Mixing increases the entropy of the liquid state and lowers the thermodynamic driving force for crystallization as well as the kinetic fragility of the system. This enables the fabrication of homogeneous thin films without any additives. In these films, the dye molecules are trapped in a glassy state, featuring monomeric absorption and emission. This strategy leads to a BODIPY material with an amorphous character in thin films, dropcast films, and bulk. Further, the strategy is based on thermodynamics and is therefore expected to be general, enabling the transformation of any dye molecule into a glass former.

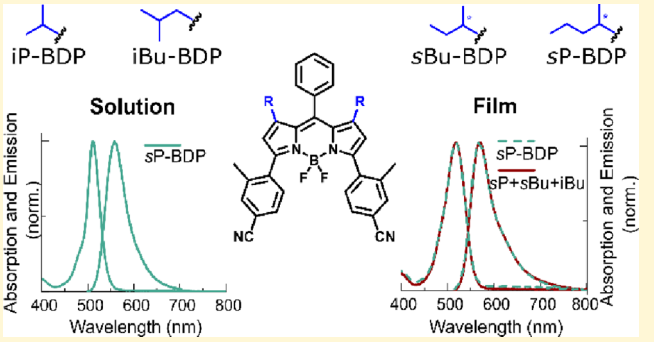

INTRODUCTION

The conversion of a material into an amorphous solid, a glass, is called vitrification. The ability of materials to vitrify is of tremendous importance for amorphous pharmaceutical formulations,[1,2] vapor-deposited glasses used in organic light-emitting diodes (OLEDs),[3−5] and also stable organic solar cells.[6−9] There is therefore a consistent high demand for designing and engineering of materials having a good glass forming ability (GFA). For photoactive materials, controlling the nanostructure of thin films is crucial for solid-state applications.[10,11] The nanostructure of a thin film highly affects the photophysical properties and with that the device performance.[12] Crystallization and aggregation lead to unwanted side effects like scattering or undesired excimer emission, and therefore a great deal of research has been devoted to controlling the thin film nanostructure and improving the GFA of photoactive materials.[13,14] Organic dyes commonly comprise a flat, aromatic core. This structural feature causes them to crystallize, promoted by intermolecular $\pi-\pi$-interactions. Strategies to reduce these interactions and prevent organic dyes from crystallizing include alkyl chain engineering, the use of additives like polymers that are mixed into the material, or by copolymerizing the dye to receive an amorphous material.[6,8,15−18] However, these methods by themselves have drawbacks, causing limitations in applicability.

To reduce $\pi-\pi$-interactions between molecules, alkylation of the π-conjugated system is a frequently used strategy. Here, a balanced interplay between the van der Waals interactions of the alkyl chains and the $\pi-\pi$-interactions of the core is targeted.[17] This strategy is mainly used in the fields of soft materials,[19] functional molecular liquids,[20] or liquid crystals.[21] It is used to control crystallization,[16,22] and can also lead to unperturbed photophysical features in films by enclosing the π-core to shield it from its environment.[20] The attached alkyl chains although often surpass the π-core in molecular weight, making this strategy only applicable for concentration-independent applications.

To what extent a material is inclined to vitrify instead of crystallizing depends on the thermodynamic and kinetic factors that influence the rate of crystal nucleation as well as crystal

Received: September 8, 2022
Revised: September 23, 2022

growth.[9,23,24] To promote the glass formation of materials, one method that can be applied is the use of multicomponent mixtures. Mixing increases the entropy of the liquid state and therefore leads to a reduction of the thermodynamic driving force for crystallisation.[25−27] These mixtures contain several different components, which together form a glass. One or several of these components are often sugars or polymers.[2,9] This leads to limitations regarding the concentration of the active component in a similar manner as alkyl chain engineering. When different optically active components are mixed, the blend will adopt the combined photophysical properties of all the components, making monomeric absorption inaccessible.[28] These limitations need to be overcome to successfully make a glass having monomeric absorption and emission features.

Here we present a guideline on how to fabricate a dye glass having monomer-like absorption and emission properties as a thin film. We use BODIPY dyes, which have received a considerable amount of attention in various fields due to their versatile photophysical properties. They possess large molar absorptivity coefficients, fluorescence quantum yields close to unity, sharp absorption and emission bands, and high photostability.[29,30] The synthesis of these dyes is relatively straightforward, which makes functionalization and modification, and with this tuning of the photophysical properties possible.[31−35] Due to these properties, BODIPY dyes and their derivatives are used in a wide array of fields such as biological imaging,[36−39] sensing,[40−42] potential agents for photodynamic and photothermal therapy,[43−45] solar cells,[46−49] and optoelectronics.[50−53]

In this work, we will show that a good glass forming ability at room temperature is achieved for BODIPYs when combining alkyl chain engineering and mixing several components. By adding short alkyl chains to the π-core of the molecule, the photophysical properties of the dye remain unchanged.[54] This allows for mixing of several derivatives, differing only in the alkyl substituents, without broadening the absorption and emission envelope of the processed material. Therefore, by first choosing appropriate BODIPY derivatives and then mixing them, a glassy film is obtained at room temperature. The presented strategy is based on thermodynamics and is therefore expected to be general, enabling the transformation of any dye molecule into a glass former.

EXPERIMENTAL SECTION

Synthesis. All reactions were carried out under ambient conditions unless stated differently, for example, performed under a N_2 atmosphere. Glassware was oven dried prior to use unless indicated otherwise. Common reagents, solvents, or materials were obtained from Sigma-Aldrich Chemical Co. and used without further purification. Dry solvents for reactions sensitive to moisture and/or oxygen were obtained through a solvent purifying system (inert PureSolv-MD-5). Column chromatography was performed using silica gel (VWR 40 to 63 μm) unless stated otherwise. Flash chromatography was performed on a Teledyne CombiFlash EZ prep using RediSepRf columns, normal-phase silica with a mesh size of 230 to 400, a particle size of 40 to 63 μm, and a pore size of 60 Å unless stated otherwise. ^{1}H (^{13}C) NMR spectra were recorded on a Varian 400 spectrometer (400 MHz ^{1}H; 100 MHz ^{13}C) at room temperature using $CDCl_3$ (the final products containing tetramethylsilane with 0.00 ppm as an internal reference) or DMSO-d_6 as solvent. Coupling constants (J values) are given in Hertz (Hz) and chemical shifts are reported in parts per million (ppm). 13C spectra are decoupled from 1H. Low-resolution MS was obtained from a GC/MSD system from Agilent 7820A GC System in tandem with an Agilent 5977E Mass Spectrometer. High-resolution MS was obtained from an Agilent 1290 infinity LC system equipped with an autosampler in tandem with an Agilent 6520 Accurate Mass Q-TOF LC/MS. Melting points were measured using a BÜCHI Melting Point B-545 instrument. IR spectra were recorded using an INVENIO R FT-IR from BRUKER.

The full synthesis is described in the Supporting Information. The Boc-protected Suzuki-coupling products were synthesized following a previously reported procedure.[55] To obtain differently alkylated compounds, the starting materials were changed accordingly.

General procedure for BODIPY Synthesis. Boc-protected Suzuki-coupling product (2.00 equiv) was added to the reaction vessel, which was subsequently evacuated and refilled with N_2 (3 cycles). The starting material was dissolved in dry THF (5 mL·mmol^{-1}). NaOMe (25 w % in MeOH, 0.4 mL·mmol^{-1}) was added to the reaction mixture and the reaction was stirred until full conversion of the starting material (approximately 2 h). H_2O was added to the reaction mixture and the phases were separated. The aqueous phase was extracted with diethyl ether (2 × 20 mL) and the combined organic phases were washed with brine (25 mL). The solvent was subsequently removed under reduced pressure. The product H-SCP-NH was obtained as a light-yellow oil and was directly used without further purification or analysis.

The deprotected Suzuki-coupling product (2.00 equiv) and benzaldehyde (1.00 equiv) were dissolved in DCM_{dry} (100 mL·mmol$_{benzaldehyde}^{-1}$). A catalytic amount of TFA was added to the solution and the solution was stirred until TLC showed full conversion of benzaldehyde (TLC: SiO_2 hexane/EtOAc 10% ca. 14 h). After full conversion was determined, DDQ (2.05 equiv) in DCM (10 mL·mmol$_{DDQ}^{-1}$) was added to the reaction mixture. The reaction mixture, which changed color from dark pink to dark purple, was stirred at room temperature for 1 h. Et_3N (6.5 mL·mmol$_{benzaldehyde}^{-1}$) was added to the reaction mixture, accompanied by a color change to dark red, and stirred for 30 min at room temperature. Afterward BF_3·OEt_2 (6.5 mL·mmol$_{benzaldehyde}^{-1}$) was added to the reaction mixture and the now dark purple solution was stirred overnight. H_2O was added to the reaction mixture, and the two-phase mixture was stirred for 1 h. Thereafter the phases were separated, and the organic phase was washed with H_2O (3 × 200 mL), afterward dried over Na_2SO_4, and then the solvent was removed under reduced pressure. The crude product was purified by column chromatography as specified for the single products.

***s*Bu-BDP.** The product was prepared following the general procedure for BODPIY synthesis and purified using column chromatography (1st: SiO_2 column, eluent: hexane/EtOAc 0−50%; 2nd: SiO_2 column, eluent: hexane/EtOAc 20%). The product was obtained as a red crystalline solid (1.52 g, 2.49 mmol, 83%), starting from tert-butyl 4-(*sec*-butyl)-2-(4-cyano-2-methylphenyl)-1*H*-pyrrole-1-carboxylate (6.00 mmol, 2.03 g, 2 equiv.).

^{1}H NMR (400 MHz, $CDCl_3$): δ 7.60−7.47 (m, 5H), 7.50−7.40 (m, 6H), 6.17 (s, 2H), 2.24 (s, 6H), 1.39−1.26 (m, 4H), 1.23−1.12 (m, 2H), 0.84 (dd, J = 6.5, 3.7 Hz, 6H), 0.56 (td, J = 7.1, 4.4 Hz, 6H). ^{13}C NMR (101 MHz, $CDCl_3$): δ 156.3, 154.9, 145.7, 138.3, 137.6, 134.3, 133.1, 132.0, 130.7, 129.6, 128.8, 128.6, 128.4, 128.3, 118.8, 112.5, 32.8, 32.7, 31.4, 31.3, 22.2, 22.1, 20.1, 12.2. IR: ν_{max}/cm^{-1} 2962, 2926, 2871, 2230, 1521, 1476, 1405, 1314, 1167, 1147, 1125, 1102, 1039, 829, 753. HRMS: (ESI$^+$) m/z: calcd. For $(M + H)^+$ $C_{39}H_{38}BF_2N_4$: 611.31576; found: 611.3151. mp 266 °C.

***i*Bu-BDP.** The product was prepared following the general procedure for BODPIY synthesis and purified using column chromatography (1st: SiO_2 column, eluent: hexane/EtOAc 10−20%; 2nd: SiO_2 column, eluent: pentane/EtOAc 10%). The product was obtained as a red crystalline solid (1.27 g, 2.08 mmol, 69%), starting from tert-butyl 2-(4-cyano-2-methylphenyl)-4-isobutyl-1*H*-pyrrole-1-carboxylate (6.00 mmol, 2.03 g, 2 equiv).

^{1}H NMR (400 MHz, $CDCl_3$): δ 7.64−7.51 (m, 3H), 7.51−7.40 (m, 8H), 6.12 (s, 2H), 2.25 (s, 6H), 1.54 (d, J = 6.5 Hz, 3H), 1.45 (dq, J = 14.2, 6.7 Hz, 2H), 0.60 (d, J = 6.4 Hz, 12H). ^{13}C NMR (101 MHz, $CDCl_3$): δ 154.4, 148.4, 145.7, 138.3, 137.5, 134.0, 133.1, 132.5, 130.7, 129.4, 128.8, 128.7, 128.6, 122.0, 118.8, 112.6, 37.0,

https://doi.org/10.1021/acs.chemmater.2c02761
Chem. Mater. XXXX, XXX, XXX−XXX

29.3, 22.3, 20.1. IR: ν_{max}/cm^{-1} 2957, 2927, 2869, 2230, 1521, 1476, 1404, 1302, 1153, 1121, 1069, 833, 757, 722. HRMS: (ESI$^+$) m/z: calcd. For $(M + H)^+$ $C_{39}H_{38}BF_2N_4$: 611.31576; found: 611.3150. mp 279 °C.

sP-BDP. The product was prepared following the general procedure for BODPIY synthesis and purified using column chromatography (1st: SiO_2 column, eluent: hexane/EtOAc 10−20%; 2nd: SiO_2 column, eluent: hexane/EtOAc 5−15%). The product was isolated as a red crystalline solid (872 mg, 1.37 mmol, 46%, isolated yield), starting from tert-butyl 2-(4-cyano-2-methylphenyl)-4-(pentan-2-yl)-1*H*-pyrrole-1-carboxylate (6.00 mmol, 2.11 g, 2 equiv).

^{1}H NMR (400 MHz, $CDCl_3$): δ 7.57−7.49 (m, 5H), 7.47−7.42 (m, 6H), 6.18 (s, 2H), 2.24 (s, 6H), 1.45 (h, J = 6.7 Hz, 2H), 1.33−1.21 (m, 2H), 1.20−1.09 (m, 1H), 1.08−0.97 (m, 1H), 0.83 (t, J = 6.7 Hz, 6H), 0.70 (td, J = 7.3, 5.0 Hz, 6H). ^{13}C NMR (101 MHz, $CDCl_3$): δ 156.5, 154.9, 145.6, 138.3, 137.6, 134.3, 133.1, 130.7, 129.6, 129.6, 128.6, 128.5, 128.4, 128.3, 118.8, 112.5, 40.7, 40.5, 31.1, 22.7, 22.3, 20.8, 20.1, 14.1. IR: ν_{max}/cm^{-1} 2958, 2927, 2869, 2230, 1521, 1475, 1405, 1309, 1147, 1125, 1098, 829, 757. HRMS: (ESI$^+$) m/z: calcd. For $(M + H)^+$ $C_{41}H_{42}BF_2N_4$: 639.34706; found: 639.3469. mp 132 °C.

iP-BDP. The product was prepared following the general procedure for BODPIY synthesis and purified using column chromatography (1st: SiO_2 column, eluent: hexane/EtOAc 0−50%; 2nd: SiO_2 column, eluent: DCM). The product was obtained as a red crystalline solid (1.27 g, 2.18 mmol, 73%), starting from tert-butyl 2-(4-cyano-2-methylphenyl)-4-isopropyl-1*H*-pyrrole-1-carboxylate (6.00 mmol, 1.95 g, 2 equiv).

^{1}H NMR (400 MHz, $CDCl_3$): δ 7.58−7.48 (m, 5H), 7.48−7.41 (m, 6H), 6.22 (s, 2H), 2.24 (s, 6H), 1.62 (p, J = 6.7 Hz, 2H), 0.87 (d, J = 6.7 Hz, 12H). ^{13}C NMR (101 MHz, $CDCl_3$): δ 157.2, 154.9, 145.7, 138.3, 137.6, 134.4, 133.1, 131.4, 130.7, 129.7, 128.6, 128.4, 118.8, 118.5, 112.5, 25.9, 24.5, 20.1. IR: ν_{max}/cm^{-1} 2969, 2928, 2871, 2229, 1519, 1477, 1405, 1314, 1169, 1147, 1126, 1089, 1065, 1032, 963, 829, 754. HRMS: (ESI$^+$) m/z: calcd. For $(M + H)^+$ $C_{37}H_{34}BF_2N_4$: 583.28446; found: 583.2845. mp 339 °C.

Sample Preparation. Glass substrates for films (25 × 25 mm) were precleaned by sonication for 1 h in an alkaline solution (0.5% of Hellmanex in distilled water), then rinsed with water and sonicated for 1 h in water and ethanol, respectively. To avoid any inner filter effects, which are dependent on the thickness of the films, the neat films as well as the blends were prepared to be very thin (∼10 nm). For thin neat films, solutions of the BODIPY dyes (c_{dye} = 0.5 mg mL^{-1}) in DCM were spin-coated (45 s, R.T., 1500 rpm) (Laurell) on the glass substrates. For thin blended films, solutions of the BODIPY dyes (c_{dye} = 0.5 mg mL^{-1}) in DCM were spin-coated (45 s, R.T., 1500 rpm) (Laurell) on the glass substrates. In the blends, the ratio of the components used is 1:1 or 1:1:1. The dyes were weighed in as powders, dissolved, and the solution was stirred for 15 min prior to spin coating. For dropcasted films, solutions of the BODIPY dyes (c_{dye} = 10.0 mg mL^{-1}) in DCM (0.5 mL) were dropcasted onto a precleaned glass substrate.

Scanning Calorimetry. Differential scanning calorimetry (DSC). Measurements were performed using a Mettler Toledo DSC2 equipped with a Gas controller GC 200 with a heating and cooling rate of 0.17 K s^{-1} (10 °C min^{-1}). Around 2−5 mg of materials was collected into 40 μL DSC Al crucibles. Fast scanning calorimetry (FSC). Measurements were carried out using a Mettler Toledo Flash DSC 1. Solutions were prepared and drop cast on glass slides. A small amount of material was transferred from the glass slide to the FSC sensor. Samples were first heated to above T_m for each material and then cooled to 25 °C with cooling rates ranging from −0.1 to −1000 K s^{-1}, followed by heating again at 2000 K s^{-1}. Two different methods were used to calculate the fictive temperatures, T_f', for the fragility plot (Figure S4). Moynihan's method was used if T_f' was above the $T_{g,onset}$, and it is calculated according to

$$\int_{T_f'}^{T\gg T_g} (C_{pl} - C_{pg})dT = \int_{T\ll T_g}^{T\gg T_g} (C_p - C_{pg})dT$$

where C_{pl} and C_{pg} are the heat capacities of the liquid and the glass, respectively, and C_p is the apparent heat capacity of the sample. If T_f' instead was below the $T_{g,onset}$, a simplified extrapolation version was used: $\int_{T_f'}^{T\gg T_g} (C_{pl} - C_{pg})dT = 0$.

Optical Spectroscopy. Absorption spectra were measured using a spectrophotometer (LAMBDA 950, PerkinElmer). Steady-state emission spectra, excitation spectra, and emission lifetimes were measured with a spectrofluorometer (FLS1000, Edinburgh Instrument) and are corrected using the emission correction files provided by the manufacturer. The emission spectra were first converted to the energy scale using the lambda-squared correction for the emission maximum when assessing the Stokes shift. The fluorescence quantum yields of samples in solution were calculated using the relative method, using a standard (fluorescein) with a known emission quantum yield.[56] Fluorescein in 0.1 M NaOH (Φ_f = 0.91) was used as a reference compound for Φ_f determination. (Excitation at 480 nm, refractive index: 1.33). The samples were measured in toluene solution at 22 °C, refractive index: 1.497. For the emission lifetime measurements, the samples were excited by a 510 nm picosecond pulsed diode laser (Edinburgh Instruments). The internal response function (IRF) was measured using a soap and water solution having a high scattering effect for samples in solution, and an Al mirror for films. Emission quantum yields of the solid samples were measured using the spectrofluorometer (FLS1000, Edinburgh Instrument) equipped with an integrating sphere. As a reference, a blank glass substrate was used.

Optical Microscopy. Optical micrographs were recorded with a Zeiss Axioscope 5 equipped with a pair of crossed polarizers.

Grazing-Incidence Wide-angle X-ray Scattering (GIWAXS). GIWAXS data were obtained on a Mat/Nordic SAXSLAB instrument. The detector used was a Pilatus3 300K R from Dectris, and the source was a Rigaku Micromax-003 with a Cu target. All measurements were carried out at a pressure of approximately 0.1 mbar in the entire flightpath. The sample to detector distance was set to 127 mm, and the incidence angle was set to 0.2°. Exposure times were 5 min. Before each measurement, a calibration of the sample tilt was performed with a z-scan and a rocking curve.

RESULTS AND DISCUSSION

Molecular Design and Synthesis. To fabricate a dye glass, the first thing one should pay careful consideration to is the design of the molecules used in the film. As mentioned previously, to prevent crystallization, $\pi-\pi$-interactions must be minimized or eliminated. Adding alkyl chains to the core structure is a commonly used strategy to counteract these $\pi-\pi$-interactions.[17,21] Branched alkyl chains have been shown to be more efficient in increasing solubility and interfering with aggregation.[54,57,58] In our molecular design, we decided to attach small but relatively bulky side chains at the 1,7-positions of the BODIPY core, shown in Figure 1. We chose branched alkyl chains of increasing length, isopropyl (iP), isobutyl (iBu), *sec*-butyl (*s*Bu) and *sec*-pentyl (*s*P). The *s*Bu and *s*P chains, in addition to being relatively bulky, introduce a stereogenic center, which means a racemic mixture of the BODIPY will be obtained. A mixture of isomers will already increase the entropy in the system compared to enantiopure compounds and will therefore be beneficial to prevent aggregation.[54] Para-cyanophenyl groups at positions 3,5 were attached in order for the compounds to be appropriate for thermal analysis. This is important since the molecule sublimates before melting if the molecular weight is too low, which we observed for compounds having only the phenyl rings without a −CN group (Figure S1). Furthermore, ortho-methyl groups on the

https://doi.org/10.1021/acs.chemmater.2c02761
Chem. Mater. XXXX, XXX, XXX−XXX

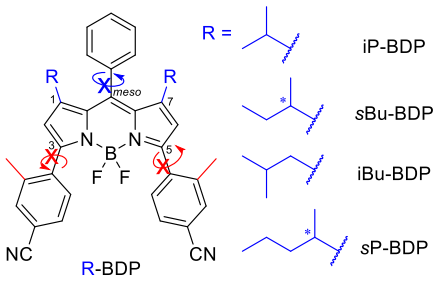

Figure 1. Structure of the designed and synthesized BODIPY derivatives, with the different alkyl chains shown in blue.

para-cyanophenyl rings in the 3,5-positions prevent planarization by blocking the rotation around the C−C bond, as indicated in Figure 1, and therefore make the molecule less prone to crystallize. The phenyl group on the meso-methine bridge was added for synthetic convenience. The planarization of this ring is blocked by the small alkyl chains in the 1,7-positions, which further reduces the crystallization potential of the molecules.

The different BODIPY derivatives were synthesized from pyrroles, carrying different alkyl chains at the 3-position, and benzaldehyde. The alkylated pyrroles were obtained via a Wittig reaction of triethyl phosphonoacetate and the corresponding aldehyde. This was followed by a Van-Leusen reaction using *p*-toluenesulfonylmethyl isocyanide (TosMIC) to form the alkylated pyrrole carboxylate esters and subsequently decarboxylation to the alkylated pyrroles. The boronic acids of the alkylated pyrroles were synthesized and coupled to 4-bromo-3-methylbenzonitrile via a Suzuki-Miyaura coupling reaction.[55] To obtain the BODIPYs, previously reported synthetic strategies were followed.[59,60] The synthesized pyrroles, together with benzaldehyde, were first submerged to condensation in the presence of a catalytic amount of trifluoroacetic acid to form the dipyrromethane. This was subsequently treated with the oxidant 2,3-dichloro-5,6-dicyano-*p*-benzoquinone (DDQ) to form the dipyrromethene, and finally, Et_3N followed by $BF_3{\cdot}OEt_2$ were added for complexation to finalize the BODIPY structure.

Neat Materials in Solution and Solid State. Following the synthesis, the derivatives were first analyzed spectroscopically to obtain information about their photophysical properties. The BODIPY derivatives can be expected to have similar photophysical properties since the only structural changes within them are the alkyl chains attached to the core structure. The derivatives in solution show as predicted highly similar absorption and emission features as shown in Table 1, Figures 2a and S7, with absorption and emission maxima at 511 and

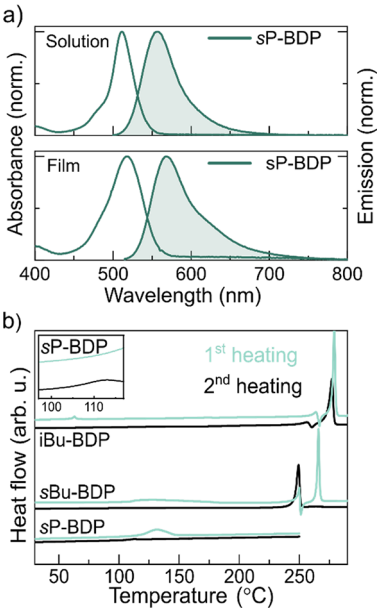

Figure 2. (a) BODIPY absorbance and emission in solution and solid state, here represented by *s*P-BDP (see Figures S7 and S8a,b for other BODIPY derivatives) (b) differential scanning calorimetry (DSC) first (green) and second (black) heating thermograms of iBu-BDP, *s*Bu-BDP and *s*P-BDP measured at a heating rate of 0.17 K s^{-1}. With a zoom on the T_g of *s*P-BDP at 110 °C in the second heating curve.

558 nm, respectively, and molar absorptivity coefficients of 61.000 to 72.000 M^{-1} cm^{-1}. The fluorescence quantum yields (Φ_f) are lower than those common for BODIPYs. The *s*Bu-BDP without the phenyl group in the meso-position is reported to have a close to unity emission quantum yield.[55] A reduced emission quantum yield through a rotating phenyl substituent in the meso position has been described previously.[60,61] Yet, methyl groups at the 1,7-positions are commonly sufficient to block the free rotation. Therefore, the drop in Φ_f is unexpected and can only be attributed to the movement of the alkyl chains and phenyl group that seemingly affect the non-radiative pathway in different amounts. For

Table 1. Spectroscopic Data of the BODIPY Derivatives in Toluene Solution at Room Temperature, and of Thin Films of the BODIPY Derivatives[a]

	*s*Bu-BDP		*s*P-BDP		iBu-BDP		iP-BDP	
	solution	Film	solution	film	solution	film	solution	film
λ_{max}Abs [nm]	511	518	511	518	513	519	511	518
λ_{max}Em [nm]	558	568	558	568	559	571	558	572
λ_{max}Exc [nm]	512	515	512	517	513	517	512	516
Stokes shift [cm^{-1}]	1646	1699	1646	1755	1604	1755	1646	1822
ε [$M^{-1}cm^{-1}$]	66600		68500		61500		72000	
Φ_f	0.29[b]	0.10[c]	0.33[b]	0.11[c]	0.48[b]	0.07[c]	0.15[b]	0.07[c]
τ_f [ns]	1.45	2.04 (0.995)[d]	1.52	1.98 (0.993)[d]	2.27	2.26 (0.991)[d]	0.76	0.86 (0.962)[d]
τ_f_2 [ns]		10.38 (0.005)[d]		9.19 (0.007)[d]		12.11 (0.009)[d]		5.31 (0.038)[d]

[a]The films were spin coated from DCM (0.5 g L^{-1}). [b]Fluorescein in 0.1 M NaOH (Φ_f = 0.91) was used as a reference compound for Φ_f determination.[56] (Excitation at 491 nm, Refractive index: 1.33). [c]Quantum yields of the films were measured using an integrating sphere. [d]Pre-exponential factors.

https://doi.org/10.1021/acs.chemmater.2c02761
Chem. Mater. XXXX, XXX, XXX−XXX

future solid-state studies, the divergent fluorescence lifetimes are, however, not of importance since movements such as rotations are likely blocked in the solid state. Thus, to summarize, the absorption and emission features of the four derivatives are close to indistinguishable. This makes them suitable candidates for mixing, which will be discussed later.

To explore how the single derivatives behave in the solid state, thin films of the dyes were fabricated (thickness ∼10 nm) and the photophysical properties were evaluated. These thin films were fabricated by spincoating of a dilute solution of the dye in DCM (0.5 g L^{-1}). The spectroscopic evaluation of the thin films is summarized in Table 1 and Figures S8a,b, S12, and S14. The thin films exhibit monomeric absorption and emission envelopes, as shown in Figure 2a, with a slight shift in absorption and emission maxima of 7−8 and 10−14 nm, respectively, in comparison to the dyes in toluene solution. This shift can be attributed to the change in environment of the dye molecules in the solid state as compared to the solution state. A polarity dependence of the absorbance maximum can also be observed when the *s*P-BDP is measured in different solvents (Figure S9). The fluorescence quantum yields drop to 7−11%. Instead of one distinct fluorescence lifetime, there is now a second, longer lifetime detected, although this one only contributes to the emission to a minor extent. The films are homogeneous and show no sign of crystallization or aggregation when analyzed with an optical microscope equipped with cross polarizers. This glass state of the films could be a result of their being too thin to provide a sufficient area density of nucleation sites for the material to crystallize. Alternatively, the glass state can be a result of the processing method. Spincoating leads to the rapid removal of the processing solvent, preventing the crystallization of the material. Anyhow, the conditions for crystallization are absent, and the molecules can therefore be considered kinetically trapped in a glass state. This would also explain the broadening of the absorption. It is most likely due to the conformational restrictions of the dyes in the film. Observations of the iP-BDP thin film over several days show an abrupt change in both absorption and emission features (Figure S10a). The very distinct broadening of the absorption peak as well as the emerging of a second emission band at around 620 nm indicate that aggregation of the molecules in the thin film occurs over time in a cooperative manner.

To further evaluate the crystallization behavior of the single materials, thick films (about 3−4 μm) were made by dropcasting. In this case, the films have both more material, which should provide a higher area density of nucleation sites, and dry slower, resulting in a longer period of time during which crystallites can form. This leads to the films being less homogeneous and less smooth, yet provides the opportunity of investigating the GFA of the materials in a scenario where the molecules are less prone to get kinetically trapped. The thick films of the BODIPY derivatives show birefringent areas using polarized optical microscopy for the iP-BDP and iBu-BDP films, which indicates the presence of ordered domains (Figure S16a,b). The iP-BDP film showed clear peaks in Grazing-Incidence Wide-Angle X-ray Scattering (GIWAXS) analysis, indicating multicrystallinity of the film (Figure S18a). The *s*Bu-BDP and *s*P-BDP films, however, are more homogeneous and show no distinct birefringent areas (Figure S16c,d). This can be explained by either the ordered domains being very small, or by the nature of the alkyl chains. As mentioned before, both the *s*Bu and the *s*P chains introduce a stereogenic center into the molecule, leading to the formation of a racemic mixture. A mixture of isomers increases the entropy of the system compared to the enantiopure system. Thus, it becomes more difficult to crystallize. Amorphous dropcasted films have already been observed for a racemic mixture of sterically hindered BODIPY derivatives carrying paracyclophane units in the 3,5-positions.[62] The film formed by these derivatives was described as "not homogeneous with spots or dried droplets". Here in comparison, our films do not dewet from the surface, and in the case of *s*Bu-BDP and *s*P-BDP, transparent films without birefringent areas are formed, as can be seen in optical micrographs.

The thick films of the racemic BODIPY mixtures did not show birefringent areas, which could indicate that the molecules do not aggregate or crystallize. Typically, the crystal nucleation rate peaks close to the glass transition temperature (T_g), while the growth rate peaks close to the melting temperature (T_m). As a consequence, both rates are highly affected by the temperature dependence of the viscosity above T_g and therefore the cooling rate. How the viscosity of a liquid increases upon cooling at the T_g is described by its kinetic fragility (m).[63,64] This measure is also used to classify glass-formers into fragile and strong glass-formers.[65]

To see if the neat materials are amorphous, or can be amorphous under other processing conditions, the thermal behavior of the material needs to be measured in bulk. This will also give additional information about the glass forming abilities of the material. First, to get information about the thermal behavior of the compounds during heating, differential scanning calorimetry (DSC) was employed. IP-BDP was determined not to be appropriate for this study. Thermogravimetric analysis showed a weight loss of material in direct proximity to the melting temperature (Figure S2), and therefore, a loss of mother material cannot be avoided during the melting of this compound. Both, iBu-BDP and *s*Bu-BDP show a high T_m with peaks at 279 and 266 °C, respectively (Figure 2b). A melting peak can be seen in both heating cycles, which indicates that the materials are crystalizing again after melting. Compared to these two derivatives, *s*P-BDP shows a much lower T_m with a maximum at 132 °C. In addition to the lower T_m, melting can only be seen in the 1st but not in the 2nd heating thermogram. Instead, a glass transition in the second heating thermogram was observed with a T_g around 110 °C. The disappearance of a T_m in combination with the appearance of a T_g indicates the absence of crystallization when cooling down, thus the formation of an amorphous solid state.

To further investigate the GFA and determine its fragility, fast scanning calorimetry (FSC) was employed. Several different processes were observed within the same heating and cooling cycle, including glass transition and crystallization (Figure S5), preventing a detailed analysis of the fragility. The single derivatives are fragile and crystallize even if cooled quickly at a cooling rate of −100 K s^{-1}. To summarize, when the single material films are very thin (∼10 nm), the molecules are trapped in a glass state. Instead, for films with a thickness of about 3−4 μm, the tendency to crystallize increases. This was seen for iP and iBu-BDP, which show birefringent areas in the thick but not in thin films. Having a racemic mixture like in the case of *s*Bu-BDP and *s*P-BDP, the entropy of the system is increased, leading to less crystalline thick films. DSC measurements of the materials in bulk show a decrease in T_m for iBu-BDP, *s*Bu-BDP, and *s*P-BDP compared to iP-BDP. For *s*P-BDP, the absence of a T_m in combination with a T_g at

https://doi.org/10.1021/acs.chemmater.2c02761
Chem. Mater. XXXX, XXX, XXX−XXX

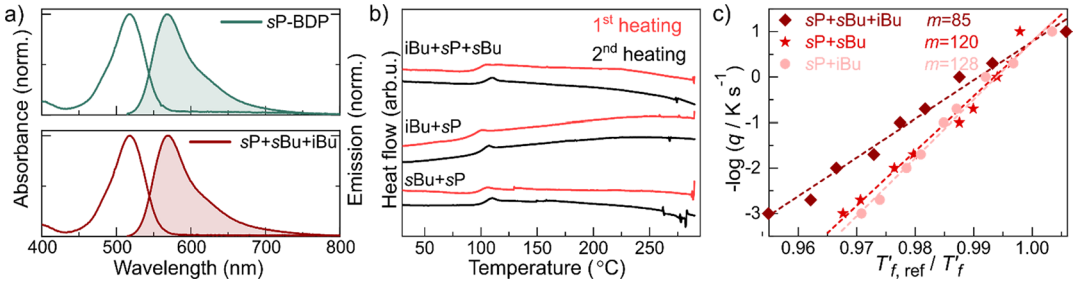

Figure 3. (a) Absorbance and emission for a *s*P-BDP film (top), representative for all neat BODIPY derivatives and the film of the ternary blend *s*P + *s*Bu + iBu (bottom), representative for all blends (Absorptivity at 518 nm = 170 ± 20 × 10^3 cm^{-1}). b) DSC first (red) and second (black) heating thermograms of iBu + *s*P + *s*Bu, iBu + *s*P and *s*Bu + *s*P measured at q = 0.17 K s^{-1} (c) Fragility plot with −log$q$ versus $T'_{f,ref}/T'_f$ of *s*P + *s*Bu + iBu (dark red squares), *s*P + *s*Bu (red stars), and *s*P + iBu (light red circles). T'_f is determined from fast scanning calorimetry (FSC) with the cooling rate q ranging from −0.1 to −1000 K s^{-1} and $T'_{f,ref}$ is measured with DSC at q = 0.17 K s^{-1}.

110 °C in the second heating thermogram indicates the formation of a glassy material.

Mixing. In applications that require an amorphous material, the glass forming ability should be as high as possible. How mixing impacts the thermodynamic driving force for crystallization depends on the change of free energy $\Delta G_{mix} = \Delta H_{mix} - T\Delta S_{mix}$ and therefore, several factors. First, the change in enthalpy upon mixing (ΔH_{mix}) has to be considered. Attractive molecular interactions between the different components, like $\pi-\pi$-interactions, can result in $\Delta H_{mix} < 0$, which can lead to a lower free energy of the mixed state and will result in a higher crystallization rate. Whereas when $\Delta H_{mix} > 0$, the free energy of the mixed state will increase and at some point, if $\Delta H_{mix} > T\Delta S_{mix}$, will not favor the mixing of the different components.[26] The type of components used is, therefore, an important factor when considering blending. Another factor is the number of different components. This naturally affects the entropy of the system upon mixing (ΔS_{mix}) and has also been shown to affect the kinetic fragility of multicomponent mixtures.[64] In the system used in this work, the components are designed to have highly similar molecular structures. Hence, this system can be considered close to ideal, and ΔH_{mix} can therefore be assumed to be close to 0. Consequently, the change of free energy $\Delta G_{mix} = \Delta H_{mix} - T\Delta S_{mix}$ depends on the change in entropy (ΔS_{mix}) of the system upon mixing.

Blending two or more of the BODIPY derivatives further increases the entropy, as compared to the racemic mixtures of *s*P- and *s*Bu-BDP, which should decrease the ability of the system to crystallize. To examine if this is applicable to our system, three binary blends and one ternary blend were made. The binary blends *s*Bu + iBu, *s*P + *s*Bu, and *s*P + iBu as well as the ternary blend *s*P + *s*Bu + iBu were made and analyzed in the same fashion as the films of neat derivatives. The DSC heating thermogram of the *s*Bu + iBu blend showed several different processes, including a glass transition at 110 °C, crystallization and melting and was therefore excluded from the study (Figure S3). All the other three blends show only one clear transition in the DSC measurements, which will be analyzed in detail further down in this section. As for the neat materials, thin films of the blends were processed by spincoating. The absorption as well as the emission transitions are of monomeric nature and are indistinguishable from the single component films as shown in Figures 3a (Figure S8c,d and Table S1). Observations of the ternary blend over time show no change in the absorption envelope. Furthermore, the emission shows the development of a small shoulder at around 620 nm over the course of several days (Figure S10b,d). As for the single component thin films, no aggregation can be observed under a polarized optical microscope. Furthermore, and importantly, the thick films (3−4 μm) fabricated by dropcasting also show no sign of birefringence (Figure S17). GIWAXS analysis shows no sign of crystallinity for the ternary blend, whereas the thick film of iP-BDP shows clear peaks (Figure S18b). This leads to the conclusion that by the mixing of BODIPY derivatives an amorphous material can be produced.

To determine if the blending of derivatives improved the GFA, first DSC was measured in bulk. The 1st and 2nd DSC heating thermograms, shown in Figure 3b, feature clear glass transitions. The T_g for all the four prepared blends has a similar value of 110 °C, and can therefore not be attributed to any specific derivative. No obvious change in the T_g can be observed by blending two or three derivatives. More noteworthy is that no melting was observed in the first heating thermograms of either of the blends. This leads to the conclusion that the material is unable to crystallize or aggregate as a result of blending the derivatives at room temperature.

Thus, it is not necessary to heat the material above the melting point in order to form an amorphous solid state, like seen in the DSC measurement of *s*P-BDP.

To determine the kinetic fragility of the blends, FSC was carried out (see Figure S4 for information on fragility calculations and Figure S6 for FSC data).[64] The binary blends have a relatively high fragility of m = 120 and m = 128 for *s*P + *s*Bu and *s*P + iBu, respectively (Figure 3c). For the ternary blend, the fragility decreased to m = 85. The ternary blend has therefore a slightly better glass forming ability than the binary blends. Furthermore, in all cases the slope is constant, indicating that no liquid−liquid transition occurs. We have previously experienced the occurrence of liquid−liquid transitions in dye glasses, leading to low fragility but also aggregation and an associated change in the emission envelope.[64] In the present study, we see no tendency of a liquid−liquid transition in the FSC data nor an aggregation associated change of the emission. The optical properties of the single molecules are conserved after mixing (Figures 3a, S8c,d, S13, and S15).

In summary, making binary and ternary blends of the BODIPY derivatives enable processing of homogeneous thin and thick films. The thin films of the multicomponent blends exhibit monomeric absorption and emission features, which are indistinguishable from the single-component thin films. DSC measurements of the blends show no melting features, which

https://doi.org/10.1021/acs.chemmater.2c02761
Chem. Mater. XXXX, XXX, XXX−XXX

indicates the creation of an amorphous solid even without erasing the thermal history by first heating over T_m. We also observed a decrease in the kinetic fragility from m = 128 to m = 85 by going from a binary to a ternary blend.

CONCLUSIONS

We presented a guideline for how to make dye materials that form an amorphous solid state as well as homogeneous thin films that exhibit monomeric absorption and emission. First and foremost, the molecular design of the single components is crucial. To block free rotation of the 1,7-phenyl substituents and decrease the potential of intermolecular $\pi-\pi$-interactions, methyl groups were attached in the ortho-position. The free rotation of the meso-phenyl substituent was blocked by attaching alkyl chains in the 3,5-positions of the BODIPY core to prevent planarization and with that $\pi-\pi$-interactions. By attaching different alkyl chains at the 3,5-positions, derivatives of the BODIPY were synthesized, which exhibit almost indistinguishable absorption and emission properties. Adding branched alkyl chains that create a stereocenter, leading to racemic mixtures, decreases the crystallization potential of the single components.

Having discussed the molecular design, the next step is the processing of the films. Spincoating, due to the rapid removal of the solvent, leads to the formation of homogeneous glassy films where the molecules get kinetically trapped into an amorphous state and no crystallization occurs. Dropcasting offers more material as well as a slower removal of the solvent. The thick films, therefore, show aggregation for iP-BDP and iBu-BDP. For *s*Bu-BDP, *s*P-BDP, both racemic mixtures, no birefringent areas were observed.

Finally, blending photophysically indistinguishable derivatives lowers the aggregation and crystallization tendency of the system. The blends prepared by spincoating result in homogeneous thin films having monomeric absorption and emission. Dropcasting of the same material results in homogeneous films without birefringent regions. The ternary blend also showed no sign of crystallinity using GIWAXS analysis. This, as well as DSC measurements, demonstrates the formation of an amorphous material without the necessity of the previous melting. In contrast, the neat materials all showed a clear T_m, and only *s*P-BDP showed a T_g. The fragility of the blends could be obtained from FSC. A decrease in the fragility of the ternary blend as compared to the binary ones was observed and the absence of a liquid−liquid transition was confirmed.

Following these steps, we prepared BODIPY materials that do not need additives to prevent crystallization and therefore solidify into a glass without any additives. This approach combines alkyl chain engineering, a method abundantly used to improve device performance and mixing of several components, to lower the crystallization tendency of the material. The here described strategy enables the formation of materials that have the potential to bring fields like optoelectronics, where dyes are used in the solid state and crystallization has so far been a limiting factor, forward.

ASSOCIATED CONTENT

Supporting Information

The Supporting Information is available free of charge at https://pubs.acs.org/doi/10.1021/acs.chemmater.2c02761.

Synthesis of the BODIPY derivatives; Wittig reaction; Van-Leusen reaction; decarboxylation toward the alkylated pyrroles and Boc-protection; synthesis of pyrrole boronic acid; Suzuki-Miyaura coupling; thermogravimetric analysis; differential scanning calorimetry; fast scanning calorimetry; normalized absorbance, excitation, and emission of the BODIPY derivatives; fluorescence lifetimes; fluorescence quantum yields; optical micrographs; grazing-incidence wide-angle X-ray scattering; ^{1}H NMR and ^{13}C NMR spectra (PDF)

AUTHOR INFORMATION

Corresponding Author

Karl Börjesson − *Department of Chemistry and Molecular Biology, University of Gothenburg, 412 96 Gothenburg, Sweden;* orcid.org/0000-0001-8533-201X; Email: karl.borjesson@gu.se

Authors

Clara Schäfer − *Department of Chemistry and Molecular Biology, University of Gothenburg, 412 96 Gothenburg, Sweden*

Sandra Hultmark − *Department of Chemistry and Chemical Engineering, Chalmers University of Technology, 412 96 Gothenburg, Sweden*

Yizhou Yang − *Department of Chemistry and Molecular Biology, University of Gothenburg, 412 96 Gothenburg, Sweden*

Christian Müller − *Department of Chemistry and Chemical Engineering, Chalmers University of Technology, 412 96 Gothenburg, Sweden;* orcid.org/0000-0001-7859-7909

Complete contact information is available at: https://pubs.acs.org/10.1021/acs.chemmater.2c02761

Author Contributions

K.B. designed the project idea. C.S., together with K.B., designed the molecules. C.S. synthesized and analyzed the molecules, prepared the films, and performed spectroscopic experiments and analysis thereof. S.H. performed DSC and FSC measurements and analyzed the resulting data together with C.M. Y.Y. measured GIWAXS. All authors contributed to writing the manuscript. All authors have given approval to the final version of the manuscript.

Funding

This research is financially supported by the Knut and Alice Wallenberg Foundation (KAW 2017.0192) and the project "Mastering Morphology for Solution Borne Electronics."

Notes

The authors declare no competing financial interest.

ACKNOWLEDGMENTS

KB acknowledges financial support from the Knut and Alice Wallenberg Foundation (KAW 2017.0192). CM acknowledges financial support from the project "Mastering Morphology for Solution Borne Electronics".

REFERENCES

(1) Qiu, Y.; Chen, Y.; Zhang, G. G. Z.; Yu, L.; Mantri, R. V.*Developing Solid Oral Dosage Forms: Pharmaceutical Theory and Practice*; Academic Press, 2017.

(2) Cicerone, M. T.; Douglas, J. F. *β*-Relaxation governs protein stability in sugar-glass matrices. *Soft Matter* **2012**, *8*, 2983−2991.

(3) Ediger, M. D. Perspective: Highly stable vapor-deposited glasses. *J. Chem. Phys.* **2017**, *147*, 210901.
(4) Tang, C. W.; VanSlyke, S. A. Organic electroluminescent diodes. *Appl. Phys. Lett.* **1987**, *51*, 913−915.
(5) Yokoyama, D. Molecular orientation in small-molecule organic light-emitting diodes. *J. Mater. Chem.* **2011**, *21*, 19187−19202.
(6) Hultmark, S.; Paleti, S. H. K.; Harillo, A.; Marina, S.; Nugroho, F. A. A.; Liu, Y.; Ericsson, L. K. E.; Li, R.; Martín, J.; Bergqvist, J.; Langhammer, C.; Zhang, F.; Yu, L.; Campoy-Quiles, M.; Moons, E.; Baran, D.; Müller, C. Suppressing Co-Crystallization of Halogenated Non-Fullerene Acceptors for Thermally Stable Ternary Solar Cells. *Adv. Funct. Mater.* **2020**, *30*, 2005462.
(7) Yu, L.; Zhang, M.; Tang, J.; Li, R.; Xu, X.; Peng, Q. Wide Bandgap Perylene Diimide Derivatives as an Effective Third Component for Parallel Connected Ternary Blend Polymer Solar Cells. *Chem. Mater.* **2021**, *33*, 7396−7407.
(8) Liu, X.; Liang, Z.; Du, S.; Tong, J.; Li, J.; Zhang, R.; Shi, X.; Yan, L.; Bao, X.; Xia, Y. Non-Halogenated Polymer Donor-Based Organic Solar Cells with a Nearly 15% Efficiency Enabled by a Classic Ternary Strategy. *ACS Appl. Energy Mater.* **2021**, *4*, 1774−1783.
(9) Müller, C. On the Glass Transition of Polymer Semiconductors and Its Impact on Polymer Solar Cell Stability. *Chem. Mater.* **2015**, *27*, 2740−2754.
(10) Singh, R.; Suranagi, S. R.; Kumar, M.; Shukla, V. K.*Mixed Solvent Engineering to Optimize Morphology and Optical Properties of Perovskite Thin Films for an Efficient Solar Cell*; Springer International Publishing: Cham, 2019, pp 309−313.
(11) Liu, Y.; Yangui, A.; Zhang, R.; Kiligaridis, A.; Moons, E.; Gao, F.; Inganäs, O.; Scheblykin, I. G.; Zhang, F. In Situ Optical Studies on Morphology Formation in Organic Photovoltaic Blends. *Small Methods* **2021**, *5*, 2100585.
(12) Yuan, L.; Lou, M.; Clark, B. D.; Lou, M.; Zhou, L.; Tian, S.; Jacobson, C. R.; Nordlander, P.; Halas, N. J. Morphology-Dependent Reactivity of a Plasmonic Photocatalyst. *ACS Nano* **2020**, *14*, 12054−12063.
(13) Riera-Galindo, S.; Tamayo, A.; Mas-Torrent, M. Role of Polymorphism and Thin-Film Morphology in Organic Semiconductors Processed by Solution Shearing. *ACS Omega* **2018**, *3*, 2329−2339.
(14) Weng, K.; Ye, L.; Zhu, L.; Xu, J.; Zhou, J.; Feng, X.; Lu, G.; Tan, S.; Liu, F.; Sun, Y. Optimized active layer morphology toward efficient and polymer batch insensitive organic solar cells. *Nat. Commun.* **2020**, *11*, 2855.
(15) Quach, J. Q.; McGhee, K. E.; Ganzer, L.; Rouse, D. M.; Lovett, B. W.; Gauger, E. M.; Keeling, J.; Cerullo, G.; Lidzey, D. G.; Virgili, T. Superabsorption in an organic microcavity: Toward a quantum battery. *Sci. Adv.* **2022**, *8*, No. eabk3160.
(16) Mo, D.; Chen, H.; Zhou, J.; Tang, N.; Han, L.; Zhu, Y.; Chao, P.; Lai, H.; Xie, Z.; He, F. Alkyl chain engineering of chlorinated acceptors for elevated solar conversion. *J. Mater. Chem. A* **2020**, *8*, 8903−8912.
(17) Lu, F.; Nakanishi, T. Alkyl-π engineering in state control toward versatile optoelectronic soft materials. *Sci. Technol. Adv. Mater.* **2015**, *16*, 014805.
(18) Zhang, T.; Ma, X.; Tian, H. A facile way to obtain near-infrared room-temperature phosphorescent soft materials based on Bodipy dyes. *Chem. Sci.* **2020**, *11*, 482−487.
(19) Li, H.; Babu, S. S.; Turner, S. T.; Neher, D.; Hollamby, M. J.; Seki, T.; Yagai, S.; Deguchi, Y.; Möhwald, H.; Nakanishi, T. Alkylated-C 60 based soft materials: regulation of self-assembly and optoelectronic properties by chain branching. *J. Mater. Chem. C* **2013**, *1*, 1943−1951.
(20) Ghosh, A.; Nakanishi, T. Frontiers of solvent-free functional molecular liquids. *Chem. Commun.* **2017**, *53*, 10344−10357.
(21) Lu, F.; Takaya, T.; Iwata, K.; Kawamura, I.; Saeki, A.; Ishii, M.; Nagura, K.; Nakanishi, T. A guide to design functional molecular liquids with tailorable properties using pyrene-fluorescence as a probe. *Sci. Rep.* **2017**, *7*, 3416.
(22) Liu, Q.; Chavhan, S.; Zhang, H.; Sun, H.; Brock, A. J.; Manzhos, S.; Chen, Y.; Feron, K.; Bottle, S. E.; McMurtrie, J. C.; Jou, J.-H.; Chen, H.-S.; Nagar, M. R.; Hu, W.; Noh, Y.-Y.; Zhen, Y.; Sonar, P. Short Alkyl Chain Engineering Modulation on Naphthalene Flanked Diketopyrrolopyrrole toward High-Performance Single Crystal Transistors and Organic Thin Film Displays. *Adv. Electron. Mater.* **2021**, *7*, 2000804.
(23) Zhao, Y.; Bian, X.; Qin, X.; Qin, J.; Hou, X. Liquid structure: Is it directly correlative to glass-forming ability? *Phys. Lett. A* **2007**, *367*, 364−368.
(24) Xie, R.; Weisen, A. R.; Lee, Y.; Aplan, M. A.; Fenton, A. M.; Masucci, A. E.; Kempe, F.; Sommer, M.; Pester, C. W.; Colby, R. H.; Gomez, E. D.Glass transition temperature from the chemical structure of conjugated polymers. *Nat. Commun.***2020**, *11*(). DOI: 10.1038/s41467-020-14656-8
(25) Kushwaha, K.; Yu, L.; Stranius, K.; Singh, S. K.; Hultmark, S.; Iqbal, M. N.; Eriksson, L.; Johnston, E.; Erhart, P.; Müller, C.; Börjesson, K. A Record Chromophore Density in High-Entropy Liquids of Two Low-Melting Perylenes: A New Strategy for Liquid Chromophores. *Adv. Sci.* **2019**, *6*, 1801650.
(26) de Zerio, A. D.; Müller, C. Glass forming acceptor alloys for highly efficient and thermally stable ternary organic solar cells. *Adv. Energy Mater.* **2018**, *8*, 1702741.
(27) Bell, I. H.; Dyre, J. C.; Ingebrigtsen, T. S. Excess-entropy scaling in supercooled binary mixtures. *Nat. Commun.* **2020**, *11*, 4300.
(28) Wu, Q.; Zhao, D.; Schneider, A. M.; Chen, W.; Yu, L. Covalently Bound Clusters of Alpha-Substituted PDI—Rival Electron Acceptors to Fullerene for Organic Solar Cells. *J. Am. Chem. Soc.* **2016**, *138*, 7248−7251.
(29) Ziessel, R.; Ulrich, G.; Harriman, A. The chemistry of Bodipy: A new El Dorado for fluorescence tools. *New J. Chem.* **2007**, *31*, 496−501.
(30) Loudet, A.; Burgess, K. BODIPY dyes and their derivatives: syntheses and spectroscopic properties. *Chem. Rev.* **2007**, *107*, 4891−4932.
(31) Ulrich, G.; Ziessel, R.; Harriman, A. The chemistry of fluorescent bodipy dyes: versatility unsurpassed. *Angew. Chem., Int. Ed. Engl.* **2008**, *47*, 1184−1201.
(32) Boens, N.; Verbelen, B.; Ortiz, M. J.; Jiao, L.; Dehaen, W. Synthesis of BODIPY dyes through postfunctionalization of the boron dipyrromethene core. *Coord. Chem. Rev.* **2019**, *399*, 213024.
(33) Xuan, S.; Zhao, N.; Ke, X.; Zhou, Z.; Fronczek, F. R.; Kadish, K. M.; Smith, K. M.; Vicente, M. G. H. Synthesis and Spectroscopic Investigation of a Series of Push−Pull Boron Dipyrromethenes (BODIPYs). *J. Org. Chem.* **2017**, *82*, 2545−2557.
(34) Tao, J.; Sun, D.; Sun, L.; Li, Z.; Fu, B.; Liu, J.; Zhang, L.; Wang, S.; Fang, Y.; Xu, H. Tuning the photo-physical properties of BODIPY dyes: Effects of 1, 3, 5, 7- substitution on their optical and electrochemical behaviours. *Dyes Pigm.* **2019**, *168*, 166−174.
(35) Zhao, W.; Xiao, F.; Jin, G.; Li, B. Design, synthesis and photophysical studies of BODIPY-o, m, p-phenylenediamine-based probes: Insights into their responsiveness under different pH conditions. *Spectrochim. Acta A Mol. Biomol. Spectrosc.* **2021**, *262*, 120118.
(36) Zhang, P. L.; Wang, Z. K.; Chen, Q. Y.; Du, X.; Gao, J. Biocompatible G-Quadruplex/BODIPY assembly for cancer cell imaging and the attenuation of mitochondria. *Bioorg. Med. Chem. Lett.* **2019**, *29*, 1943−1947.
(37) Zhu, X.-Y.; Yao, H.-W.; Fu, Y.-J.; Guo, X.-F.; Wang, H. Effect of substituents on Stokes shift of BODIPY and its application in designing bioimaging probes. *Anal. Chim. Acta* **2019**, *1048*, 194−203.
(38) Shi, Z.; Han, X.; Hu, W.; Bai, H.; Peng, B.; Ji, L.; Fan, Q.; Li, L.; Huang, W. Bioapplications of small molecule Aza-BODIPY: from rational structural design to in vivo investigations. *Chem. Soc. Rev.* **2020**, *49*, 7533−7567.
(39) Nguyen, V.-N.; Ha, J.; Cho, M.; Li, H.; Swamy, K. M. K.; Yoon, J. Recent developments ofBODIPY-based colorimetric and fluorescent probes for the detection of reactive oxygen/nitrogen species and cancer diagnosis. *Coord. Chem. Rev.* **2021**, *439*, 213936.

(40) Thivierge, C.; Han, J.; Jenkins, R. M.; Burgess, K. Fluorescent proton sensors based on energy transfer. *J. Org. Chem.* **2011**, *76*, 5219−5228.
(41) Raut, S.; Kimball, J.; Fudala, R.; Doan, H.; Maliwal, B.; Sabnis, N.; Lacko, A.; Gryczynski, I.; Dzyuba, S. V.; Gryczynski, Z. A homodimeric BODIPY rotor as a fluorescent viscosity sensor for membrane-mimicking and cellular environments. *Phys. Chem. Chem. Phys.* **2014**, *16*, 27037−27042.
(42) Ozcan, E.; Kazan, H. H.; Çoşut, B. Recent chemo-/biosensor and bioimaging studies based on indole-decorated BODIPYs. *Luminescence* **2020**, *35*, 168−177.
(43) Kamkaew, A.; Lim, S. H.; Lee, H. B.; Kiew, L. V.; Chung, L. Y.; Burgess, K. BODIPY dyes in photodynamic therapy. *Chem. Soc. Rev.* **2013**, *42*, 77−88.
(44) Chen, D.; Wang, Z.; Dai, H.; Lv, X.; Ma, Q.; Yang, D.-P.; Shao, J.; Xu, Z.; Dong, X. Boosting O2•− Photogeneration via Promoting Intersystem-Crossing and Electron-Donating Efficiency of Aza-BODIPY-Based Nanoplatforms for Hypoxic-Tumor Photodynamic Therapy. *Small Methods* **2020**, *4*, 2000013.
(45) Rattanopas, S.; Chansaenpak, K.; Siwawannapong, K.; Ngamchuea, K.; Wet-osot, S.; Treekoon, J.; Pewklang, T.; Jinaphon, T.; Sagarik, K.; Lai, R.-Y.; Cheng, L.; Kamkaew, A. Synthesis and Characterization of Push-Pull Aza-BODIPY Dyes Towards Application in NIR-II Photothermal Therapy. *ChemPhotoChem* **2020**, *4*, 5304−5311.
(46) Klfout, H.; Stewart, A.; Elkhalifa, M.; He, H. BODIPYs for Dye-Sensitized Solar Cells. *ACS Appl. Mater. Interfaces* **2017**, *9*, 39873−39889.
(47) Srinivasa Rao, R.; Bagui, A.; Hanumantha Rao, G.; Gupta, V.; Singh, S. P. Achieving the highest efficiency using a BODIPY core decorated with dithiafulvalene wings for small molecule based solution-processed organic solar cells. *Chem. Commun.* **2017**, *53*, 6953−6956.
(48) Gkini, K.; Verykios, A.; Balis, N.; Kaltzoglou, A.; Papadakis, M.; Adamis, K. S.; Armadorou, K.-K.; Soultati, A.; Drivas, C.; Gardelis, S.; Petsalakis, I. D.; Palilis, L. C.; Fakharuddin, A.; Haider, M. I.; Bao, X.; Kennou, S.; Argitis, P.; Schmidt-Mende, L.; Coutsolelos, A. G.; Falaras, P.; Vasilopoulou, M. Enhanced Organic and Perovskite Solar Cell Performance through Modification of the Electron-Selective Contact with a Bodipy−Porphyrin Dyad. *ACS Appl. Mater. Interfaces* **2020**, *12*, 1120−1131.
(49) Chen, J. J.; Conron, S. M.; Erwin, P.; Dimitriou, M.; McAlahney, K.; Thompson, M. E. High-Efficiency BODIPY-Based Organic Photovoltaics. *ACS Appl. Mater. Interfaces* **2015**, *7*, 662−669.
(50) Squeo, B. M.; Gregoriou, V. G.; Avgeropoulos, A.; Baysec, S.; Allard, S.; Scherf, U.; Chochos, C. L. BODIPY-based polymeric dyes as emerging horizon materials for biological sensing and organic electronic applications. *Prog. Polym. Sci.* **2017**, *71*, 26−52.
(51) Poddar, M.; Misra, R. Recent advances of BODIPY based derivatives for optoelectronic applications. *Coord. Chem. Rev.* **2020**, *421*, 213462.
(52) Chapran, M.; Angioni, E.; Findlay, N. J.; Breig, B.; Cherpak, V.; Stakhira, P.; Tuttle, T.; Volyniuk, D.; Grazulevicius, J. V.; Nastishin, Y. A.; Lavrentovich, O. D.; Skabara, P. J. An Ambipolar BODIPY Derivative for a White Exciplex OLED and Cholesteric Liquid Crystal Laser toward Multifunctional Devices. *ACS Appl. Mater. Interfaces* **2017**, *9*, 4750−4757.
(53) Squeo, B. M.; Pasini, M. BODIPY platform: a tunable tool for green to NIR OLEDs. *Supramol. Chem.* **2020**, *32*, 56−70.
(54) Schäfer, C.; Mony, J.; Olsson, T.; Börjesson, K. Entropic Mixing Allows Monomeric-Like Absorption in Neat BODIPY Films. *Chem. Eur. J.* **2020**, *26*, 14295−14299.
(55) Schäfer, C.; Mony, J.; Olsson, T.; Börjesson, K. Effect of the Aza-N-Bridge and Push−Pull Moieties: A Comparative Study between BODIPYs and Aza-BODIPYs. *J. Org. Chem.* **2022**, *87*, 2569−2579.
(56) Brouwer, A. M. Standards for photoluminescence quantum yield measurements in solution (IUPAC Technical Report). *Pure Appl. Chem.* **2011**, *83*, 2213−2228.
(57) Ozdemir, T.; Atilgan, S.; Kutuk, I.; Yildirim, L. T.; Tulek, A.; Bayindir, M.; Akkaya, E. U. Solid-State Emissive BODIPY Dyes with Bulky Substituents As Spacers. *Org. Lett.* **2009**, *11*, 2105−2107.
(58) Hollamby, M. J.; Nakanishi, T. The power of branched chains: optimising functional molecular materials. *J. Mater. Chem. C* **2013**, *1*, 6178−6183.
(59) Maity, A.; Ghosh, U.; Giri, D.; Mukherjee, D.; Maiti, T. K.; Patra, S. K. A water-soluble BODIPY based 'OFF/ON' fluorescent probe for the detection of Cd2+ ions with high selectivity and sensitivity. *Dalton Trans.* **2019**, *48*, 2108−2117.
(60) Duan, C.; Zhou, Y.; Shan, G.-G.; Chen, Y.; Zhao, W.; Yuan, D.; Zeng, L.; Huang, X.; Niu, G. Bright solid-state red-emissive BODIPYs: facile synthesis and their high-contrast mechanochromic properties. *J. Mater. Chem. C* **2019**, *7*, 3471−3478.
(61) Hu, R.; Lager, E.; Aguilar-Aguilar, A.; Liu, J.; Lam, J. W. Y.; Sung, H. H. Y.; Williams, I. D.; Zhong, Y.; Wong, K. S.; Peña-Cabrera, E.; Tang, B. Z. Twisted Intramolecular Charge Transfer and Aggregation-Induced Emission of BODIPY Derivatives. *J. Phys. Chem. C* **2009**, *113*, 15845−15853.
(62) Vu, T. T.; Badré, S.; Dumas-Verdes, C.; Vachon, J.-J.; Julien, C.; Audebert, P.; Senotrusova, E. Y.; Schmidt, E. Y.; Trofimov, B. A.; Pansu, R. B.; Clavier, G.; Méallet-Renault, R. New Hindered BODIPY Derivatives: Solution and Amorphous State Fluorescence Properties. *J. Phys. Chem. C* **2009**, *113*, 11844−11855.
(63) Mauro, N. A.; Blodgett, M.; Johnson, M. L.; Vogt, A. J.; Kelton, K. F. A structural signature of liquid fragility. *Nat. Commun.* **2014**, *5*, 4616.
(64) Hultmark, S.; Cravcenco, A.; Kushwaha, K.; Mallick, S.; Erhart, P.; Börjesson, K.; Müller, C. Vitrification of octonary perylene mixtures with ultralow fragility. *Sci. Adv.* **2021**, *7*, No. eabi4659.
(65) Kelton, K. F. Kinetic and structural fragility—a correlation between structures and dynamics in metallic liquids and glasses. *J. Phys.: Condens. Matter* **2016**, *29*, 023002.

https://doi.org/10.1021/acs.chemmater.2c02761
Chem. Mater. XXXX, XXX, XXX−XXX